Automatica 173 (2025) 112092

Contents lists available at ScienceDirect

Automatica

journal homepage: www.elsevier.com/locate/automatica

Brief paper

# State estimation of solid-state batteries via a distributed parameter electrochemical model ☆

Dong Zhang [a], Shu-Xia Tang [b,*], Luis D. Couto [c], Zhongbao Wei [d], Venkatasubramanian Viswanathan [e]

[a] School of Aerospace and Mechanical Engineering, University of Oklahoma, Norman, OK, USA
[b] Department of Mechanical Engineering, Texas Tech University, Lubbock, TX, USA
[c] Vlaamse Instelling voor Technologisch Onderzoek (VITO), Unit Energy Technology, B-2400 Mol, Belgium
[d] National Engineering Laboratory for Electric Vehicles, School of Mechanical Engineering, Beijing Institute of Technology, China
[e] Department of Aerospace Engineering, University of Michigan, Ann Arbor, MI, USA

ARTICLE INFO

*Article history:*
Received 18 June 2022
Received in revised form 8 June 2024
Accepted 18 November 2024
Available online 13 January 2025

*Keywords:*
Solid-state battery
Electrochemical model
State estimation
Semilinear PDE observer

ABSTRACT

Solid-state Lithium-ion (Li-ion) batteries have emerged to be one of the leading candidates for future energy storage systems owing to their exceptional high specific energy and safety benefits. Accurate electrochemical information enables safe and optimal energy management. This paper presents a provably convergent partial differential equation (PDE) based state estimation framework utilizing an electrochemical solid-state battery model, by leveraging voltage and current measurements only. Notably, this work promptly considers various crucial nonlinear effects and electrolyte dynamics. In particular, the nonlinear generation/recombination process of Li-ions in the solid electrolyte is pivotal in predicting electrolyte Li-ion distributions. We develop a robust state observer by exploiting concepts from semilinear PDE backstepping technique without relying on prior model discretization and reduction. The estimation error stability and input-to-state stability are also rigorously demonstrated.

© 2024 Elsevier Ltd. All rights are reserved, including those for text and data mining, AI training, and similar technologies.

## 1. Introduction

Autonomy is crucial for applications like electric vehicles (EVs). This feature has been enabled by lithium-ion (Li-ion) batteries, which benefit from high energy and power densities and prolonged service life. However, safety concerns persists due to their propensity to failure, including overcharging and thermal/mechanical abuses. The electrification of other sectors such as long-haul trucks and aviation also promotes the quest for pushing the batteries performance envelope towards even higher energy densities. Among the potentially promising next-generation battery candidates, solid-state Li-ion batteries offer higher energy density and better thermal stability (Janek & Zeier, 2023). Solid-state batteries work similarly as liquid-electrolyte-based batteries with porous electrodes, but a major distinction is the substitution of a porous electrode by Li metal in the anode and the solid electrolyte instead of a liquid one. As a result, the porous electrode theory (Doyle, Fuller, & Newman, 1993) used to model Li-ion batteries is no longer appropriate to describe metal anode as it involves plating and stripping of metallic lithium rather than intercalation and de-intercalation.

Most battery modeling research focuses on Li-ion batteries, with limited attention to solid-state batteries. Early work on solid-state battery modeling was carried out by Danilov et al. who proposed a one-dimensional framework to predict the dynamic behavior of a $Li|Li_3PO_4|LiCoO_2$ cell (Danilov, Niessen, & Notten, 2010). This model accounts for the charge transfer kinetics and diffusion and migration of ions. Kazemi et al. subsequently proposed phase-transition processes and a concentration-dependent lithium diffusivity to improve model accuracy at high currents (Kazemi et al., 2019). Furthermore, Fabre et al. developed a model for $Li|LiPON|LiCoO_2$ thin-film microbattery with a uniform concentration of lithium ions across the electrolyte (Fabre, Guy-Bouyssou, Bouillon, Le Cras, & Delacourt, 2011), while Behrou et al. introduced a finite element framework for electrochemical and mechanical interactions considering damage evolution (Behrou & Maute, 2017). Raijmakers et al. improved the model in Danilov et al. (2010) by incorporating electrical double layers and mixed ionic/electronic conductivities notably (Raijmakers, Danilov, Eichel, & Notten, 2020). Phase-field modeling has also emerged as a tool to explore mechanisms related to morphological instabilities in lithium metal anode (Ahmad, Hong, & Viswanathan, 2020). More recently, control-oriented models for

☆ The material in this paper was not presented at any conference. This paper was recommended for publication in revised form by Associate Editor Prashant Mhaskar under the direction of Editor Thomas Parisini.

* Corresponding author.
*E-mail addresses:* dzhang@ou.edu (D. Zhang), shuxia.tang@ttu.edu (S.-X. Tang), luis.coutomendonca@vito.be (L.D. Couto), weizb@bit.edu.cn (Z. Wei), venkvis@umich.edu (V. Viswanathan).

https://doi.org/10.1016/j.automatica.2024.112092
0005-1098/© 2024 Elsevier Ltd. All rights are reserved, including those for text and data mining, AI training, and similar technologies.

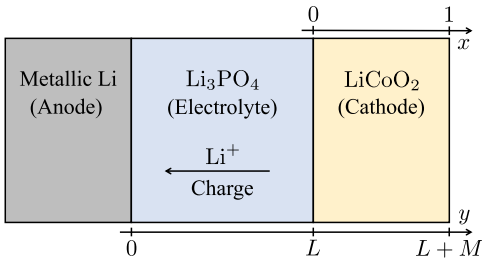


**Fig. 1.** A schematic of a thin film solid-state battery (Danilov et al., 2010).

solid-state batteries have started to emerge. Kim et al. neglected the generation/recombination of Li-ions in the electrolyte and imposed a uniform electrolyte concentration in Danilov's model (Upreti, Oyewole, Lin, & Kim, 2019). A reduced-order electrochemical model using Padé and polynomial approximations was proposed in Deng et al. (2020). In regards to state estimation, only (Deng, Hu, Lin, Kim, & Li, 2021; Kim, Lin, Abbasalinejad, Kim, & Chung, 2019) have developed observers for lithium concentrations via Kalman filters (KF). Key drawbacks of these works include: (*i*) nonlinear dynamics are often neglected, and (*ii*) the methods require a-priori spatial discretization for finite-dimensional approximation.

To tackle the gaps, we propose a partial differential equation (PDE) based observer. Prior literature exploited PDE observers for Li-ion batteries, including Single Particle Model (SPM) (Moura, Argomedo, Klein, Mirtabatabaei, & Krstic, 2016), SPM with phase transition materials (Koga, Camacho-Solorio, & Krstic, 2021), and temperature estimation (Zhang, Dey, Tang, Drummond and Moura, 2021), all of which laid the foundation for battery PDE estimation but neglected intrinsic nonlinearities or overlooked the model uncertainties. Our work extends this knowledge to solid-state batteries (Zhang, Tang, Couto, & Viswanathan, 2021) to develop

- an observer that retains the nonlinear structure of the electrochemical PDE model, therefore preserving the fidelity and physical significance of the equations;
- a backstepping observer for a class of semilinear PDEs with measurement uncertainty, which offers an input-to-state stability and ease of parameter tuning;
- a framework for model reduction and boundary state estimation to resolve weak observability issue in battery electrochemical models. We obtained reasonable transfer functions compared to the ones in Deng et al. (2020).

**Notations.** The 2-norm for a vector $\mathbf{x} = [x_1 \quad x_2 \quad \cdots \quad x_n]^\top$ is given by $\|\mathbf{x}\|_2 = \sqrt{x_1^2 + x_2^2 + \cdots + x_n^2}$. The $L_2$ norm for a function $f(z,t)$, $z \in [0,1]$, $t \in [0,\infty)$ is $\|f(\cdot,t)\| = (\int_0^1 f^2(z,t)\mathrm{d}z)^{1/2}$, and the infinity norm is $\|f(\cdot,t)\|_\infty = \sup_{z\in[0,1]} |f(z,t)|$.

## 2. Modeling for solid-state batteries

A thin film solid-state battery is considered (Fig. 1). The anode is formed by metallic lithium, and the electrodes are detached using a solid electrolyte which also plays the role of a separator. An overview of the model is presented, which assumes (i) a one-dimensional structure and (ii) the anode charge transfer kinetics are ignored (Danilov et al., 2010). Symbols used in the model are in Table 1.

**Table 1**
Solid-state battery model symbol description.

| Symbols | Description | Units |
|---|---|---|
| $A$ | Cell cross sectional area | [$m^2$] |
| $\alpha_a$, $\alpha_c$ | Charge transfer coefficients | [–] |
| $c_{Li^+}$ | $Li^+$ conc. in electrolyte | [mol/$m^3$] |
| $c_{Li^+,max}$ | Max $Li^+$ conc. in electrolyte | [mol/$m^3$] |
| $c_{Lis}$ | Li conc. in cathode | [mol/$m^3$] |
| $c_{Lis,max}$ | Max Li conc. in cathode | [mol/$m^3$] |
| $c_{Lis,min}$ | Min Li conc. in cathode | [mol/$m^3$] |
| $D_{Li^+}$ | $Li^+$ Diffusivity in electrolyte | [$m^2$/s] |
| $D_{n^-}$ | $n^-$ Diffusivity in electrolyte | [$m^2$/s] |
| $D_{Lis}$ | Li Diffusivity in cathode | [$m^2$/s] |
| $F$ | Faraday's constant | [C/mol] |
| $I$ | Applied current | [A] |
| $k_r$ | Recombination reaction rate | [$m^3$/mol-s] |
| $k_0^{app}$ | Apparent rate constant | [$m^3$/mol-s] |
| $M$ | Cathode thickness | [m] |
| $L$ | Solid electrolyte thickness | [m] |
| $R$ | Universal gas constant | [J/mol-K] |
| $T$ | Temperature | [K] |
| $t$ | Time | [s] |
| $\eta_{mt}$ | Mass transfer overpotential | [V] |
| $\eta_{ct}$ | Charge transfer overpotential | [V] |
| $\eta_d$ | Diffusion overpotential | [V] |

### 2.1. Dynamics for solid electrolyte

The transport of Li-ions in the solid electrolyte is driven by the diffusion–migration process combined with the generation/recombination reaction, the dynamics are governed by a nonlinear reaction–diffusion type system:

$$\frac{\partial c_{Li^+}}{\partial t}(y,t) = D_e \frac{\partial^2 c_{Li^+}}{\partial y^2}(y,t) + r\left(c_{Li^+}(y,t)\right), \tag{1}$$

$$\frac{\partial c_{Li^+}}{\partial y}(0,t) = -\frac{I(t)}{2FAD_{Li^+}}, \tag{2}$$

$$\frac{\partial c_{Li^+}}{\partial y}(L,t) = -\frac{I(t)}{2FAD_{Li^+}}, \tag{3}$$

$$c_{Li^+}(y,0) = \delta c_{Li^+,max}, \tag{4}$$

where $D_e = (2D_{Li^+}D_{n^-})/(D_{Li^+} + D_{n^-})$, $\delta$ denotes the fraction of mobile $Li^+$ in equilibrium, $y \in [0, L]$, and positive current denotes charging by convention. Moreover, the charge carrier generation can be expressed via

$$r\left(c_{Li^+}(y,t)\right) = \alpha c_{Li^+}^2 + \beta c_{Li^+} + \sigma, \tag{5}$$

where $\alpha = -k_r$, $\beta = -k_r\delta^2 c_{Li^+,0}/(1-\delta)$, and $\sigma = k_r\delta^2 c_{Li^+,0}/(1-\delta)$. The electrolyte dynamics (1)–(4) belong to a class of semilinear diffusion–reaction PDE with Neumann boundary conditions.

The diffusion and migration overpotentials across the solid electrolyte are the primary sources of the total mass transfer overpotential,

$$\eta_{mt}(t) = \frac{RT}{F}\ln\left[\frac{c_{Li^+}(L,t)}{c_{Li^+}(0,t)}\right] - \int_0^L E(y,t)\mathrm{d}y, \tag{6}$$

in which $E$ denotes the electric field

$$E = \frac{RT}{F}\frac{1}{c_{Li^+}}\left(-\frac{I}{2FAD_{Li^+}} + \frac{D_{Li^+} - D_{n^-}}{D_{Li^+} + D_{n^-}}\left[\frac{\partial c_{Li^+}}{\partial y} - \frac{I}{2FAD_{Li^+}}\right]\right). \tag{7}$$

### 2.2. Dynamics for cathode

When assuming $Li^+$ diffusion-induced concentration gradient is the dominating means of charge transfer, cathode lithium

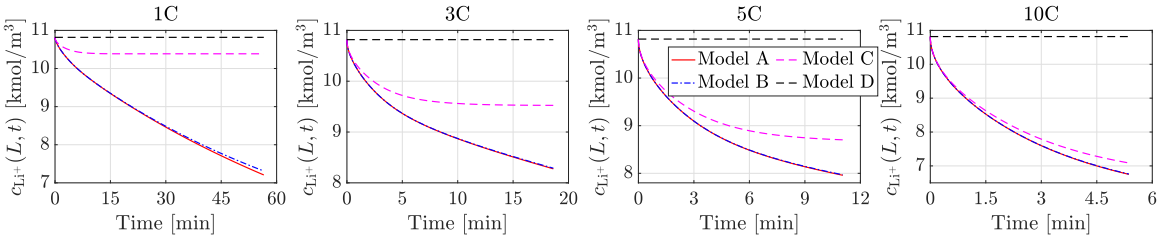


**Fig. 2.** Simulations of electrolyte concentrations at electrolyte–cathode interface for Models A-D for various discharge rates.

transport is given by the Fick's law:

$$\frac{\partial c_{\text{Lis}}}{\partial t}(y,t) = D_{\text{Lis}} \frac{\partial^2 c_{\text{Lis}}}{\partial y^2}(y,t), \tag{8}$$

$$\frac{\partial c_{\text{Lis}}}{\partial y}(L,t) = -\frac{I(t)}{FAD_{\text{Lis}}}, \tag{9}$$

$$\frac{\partial c_{\text{Lis}}}{\partial y}(L+M,t) = 0, \tag{10}$$

$$c_{\text{Lis}}(y,0) = c_{\text{Lis},0}. \tag{11}$$

The cathode dynamics (8)–(11) exemplify a class of linear parabolic PDE with Neumann boundary conditions.

The Butler–Volmer kinetics link the charge transfer overpotential for the cathode and the current via

$$I = i_0 \left[ \exp\left(\frac{\alpha_a F \eta_{\text{ct}}}{RT}\right) - \exp\left(\frac{-\alpha_c F \eta_{\text{ct}}}{RT}\right) \right], \tag{12}$$

where the exchange current density $i_0$ is a function of $c_{\text{Lis}}(L,t)$ (namely Li concentration in $LiCoO_2$ at the electrolyte–cathode interface) and $c_{\text{Li}^+}(L,t)$ (the concentration of $Li^+$ in the electrolyte at the interface) (Fabre et al., 2011):

$$i_0(t) = F \left[k_a(c_{\text{Li}^+,\max} - c_{\text{Li}^+}(L,t))c_{\text{Lis}}(L,t)\right]^{\alpha_c} \times \left[k_c(c_{\text{Lis},\max} - c_{\text{Lis}}(L,t))c_{\text{Li}^+}(L,t)\right]^{\alpha_a}. \tag{13}$$

Let $\theta(y,t) = c_{\text{Lis}}(y,t)/c_{\text{Lis},\max}$, then we have

$$\eta_d = E_{\text{eq}}(\theta_s) - E_{\text{eq}}(\bar{\theta}), \tag{14}$$

where $E_{\text{eq}}$ denotes the cathode equilibrium potential. $\theta_s(t) = \theta(L,t)$ is the normalized cathode lithium concentration at electrolyte–cathode interface, and $\bar{\theta}(t)$ is the normalized volume-averaged lithium concentration.

### 2.3. Output voltage

The total overpotential is the sum of three components: mass transfer overpotential in the electrolyte, charge transfer overpotential for the cathode, and diffusion overpotential for the cathode. Mathematically,

$$\eta_t = \eta_{\text{mt}} + \eta_{\text{ct}} + \eta_{\text{d}}, \tag{15}$$

where the terms on the right-hand side were presented in (6), (12) and (14), respectively. Ultimately, battery output voltage is dictated by the combined effects from the equilibrium voltage and the dynamic overpotentials,

$$V = E_{\text{eq}}(\bar{\theta}) + \eta_t = E_{\text{eq}}(\theta_s) + \eta_{\text{mt}} + \eta_{\text{ct}}. \tag{16}$$

## 3. Model analysis, comparison, and reduction

The model is nonlinear, particularly in the electrolyte dynamics due to the generation/recombination, exacerbated by overpotentials. This section explores model reductions towards a feasible state observer design.

### 3.1. Effects of electrolyte dynamics

We first examine the impacts of electrolyte dynamics via the comparison of four models:

- Model A: Full-order model from Section 2.
- Model B: Model A with a linearized reaction term $r$,
$$r \approx \left(\beta + 2\alpha c_{\text{Li}^+}^{\text{eq}}\right) \cdot c_{\text{Li}^+}(y,t) + \sigma - \alpha (c_{\text{Li}^+}^{\text{eq}})^2 \tag{17}$$
around an equilibrium $c_{\text{Li}^+} = c_{\text{Li}^+}^{\text{eq}}$.
- Model C: Model A excluding term $r$ in the electrolyte.
- Model D: Model A excluding electrolyte dynamics.

These four models are simulated with a 1C discharge current. The root mean squared error (RMSE) between Model A and Models B, C, and D are 0.047 mV, 0.95 mV, and 21.0 mV, respectively. Despite negligible influence of the term $r$ on voltage between Model A and C, clear bias exists in the electrolyte concentration predictions from Models C and D, as highlighted in Fig. 2. The electrolyte concentration in the full-order model trends down since the reaction $r < 0$ consumes lithium. On the contrary, Model B demonstrates improved prediction due to the preservation of the generation/recombination. The analysis exemplifies the significance of the generation/recombination since it consistently consumes lithium that could lead to lithium depletion — reaffirming the importance of electrolyte lithium concentration monitoring.

### 3.2. Effects of overpotentials

We now numerically compare voltage prediction accuracy with and without the nonlinear integral term in (6) under various current rates in Fig. 3, in which the solid lines represent full voltage model given by (16) whereas the circles denote voltage curves excluding the integral term. The RMSE between the full-order and the reduced voltage models are 2.4 mV, 6.2 mV, 9.8 mV, and 18.1 mV, respectively for 1C, 3C, 5C, and 10C discharge rates. As C-rate increases the electrolyte gradient becomes significant, thus the contribution of the electric field to the mass transfer overpotential escalates. However, even under high current rates, the integral term does not dominate the voltage prediction (Kim et al., 2019), and thus we simplify the model structure by neglecting this term. As a result, the mass transfer overpotential $\eta_{\text{mt}}$ is entirely characterized by the $Li^+$ concentrations at the electrolyte domain boundaries. Finally, by assuming $\alpha_a = \alpha_c = 0.5$, we rewrite the voltage function (16) by grouping simplified versions of overpotentials:

$$V = E_{\text{eq}}(\theta_s(t)) + \frac{RT}{F}\left[\ln c_{\text{Li}^+}(L,t) - \ln c_{\text{Li}^+}(0,t)\right] + \frac{2RT}{F}\sinh^{-1}\left[\frac{I(t)}{2i_0(c_{\text{Li}^+}(L,t), c_{\text{Lis}}(L,t))}\right]. \tag{18}$$

Henceforth, the reduced-order voltage (18) will be utilized as the plant model output function. It is worth noting that this expression is sorely determined by lithium concentrations at domain boundaries, namely $Li^+$ concentration at $y = 0, L$ and Li concentration at $y = L$.

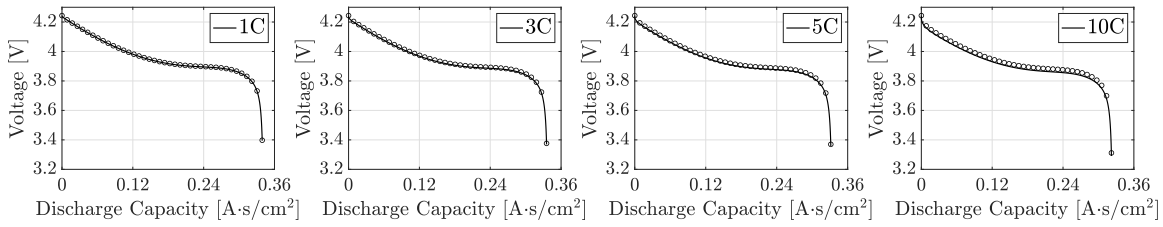


**Fig. 3.** Voltage curves across various discharge C-rates. Solid lines represent full-order voltage model calculated from (16), and circles represent voltage predictions excluding the integral term in the mass transfer overpotential (6).

## 4. State observer design and analysis

We detail the design of an observer to track the lithium concentration distribution, using voltage and current only. Traditional observers for Li-ion batteries, such as Di Domenico, Stefanopoulou, and Fiengo (2010), discrete PDE models into systems of ordinary differential equations (ODE) and then apply output-error-injection-based correction and prediction strategies, a process known as "early lumping". However, these methods often sacrifice the physical significance of the PDE models, leading to potential inaccuracies in state estimates. To address this, we will perform observer design on the PDE model without spatial discretization, a novel approach that separates this work from other finite-dimensional counterpart for solid-state batteries.

Arguably, the primary challenge in state estimation is the model's nonlinearity. Previous studies for solid-state batteries, e.g., Deng et al. (2021, 2020), and Kim et al. (2019), simplified the model by neglecting the nonlinear electrolyte dynamics. We tackle this research gap with a PDE observer using the full-order nonlinear model, including the electrolyte generation/recombination to maintain the high fidelity. Fig. 4 outlines the observer framework. The electrolyte observer (blue block) and cathode observer (yellow block) rely on their boundary states for PDE boundary error injection. However, these boundary states are not directly measured must be computed from the measured voltage and current (green block). Notably, similar task was carried out in Moura et al. (2016) by means of a voltage function inversion, but the enabling property was a locally one-to-one mapping — a sufficient condition for unique function inversion. Nevertheless, our voltage function (18) is dependent on multiple variables — making it impossible to uniquely compute individual boundary state from this single algebraic relation. A novel methodology for obtaining these domain boundary states will be proposed in Section 5.

**Remark 1.** The solid-state battery system with electrolyte and electrode dynamics are not fully observable from voltage (Hermann & Krener, 1977). The idea behind resolving the unobservability issue is to separate electrolyte voltage from that of the electrode to ensure observability in their individual domain. This framework can be generalized to resolve unobservability problem in Li-ion battery electrochemical model-based state estimation (Zhang, Couto, & Moura, 2020).

We now present a PDE observer for the nonlinear electrolyte model (1)–(4) to estimate $Li^+$ concentration in the solid electrolyte, assuming the knowledge of electrolyte boundary state $c_{Li^+}(L,t)$. First, we scale the spatial coordinate $y$ and time coordinate $t$ via $x = y/L \in [0,1]$, $\tau_e = (D_{\text{eff}}/L^2)t$, and let $w(x,\tau_e) = c_{Li^+}(y,t)$. Henceforth, without loss of generality, we will slightly abuse the notation by using $t$ (rather than $\tau_e$) for the temporal coordinate when the context is clear. This produces the following semilinear PDE with Neumann boundary conditions:

$$w_t(x,t) = w_{xx}(x,t) + f(w(x,t)), \tag{19}$$

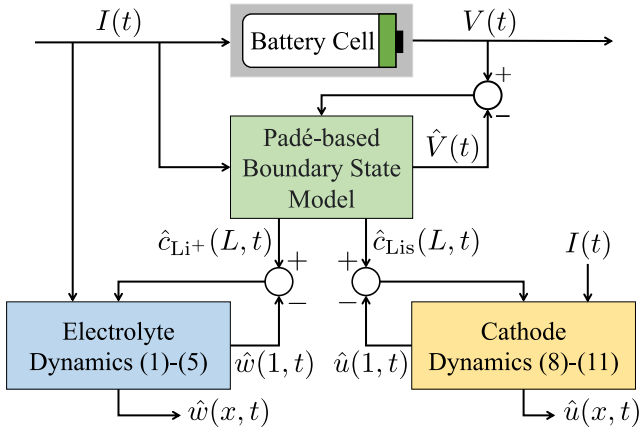


**Fig. 4.** The state observer utilizes an electrolyte PDE backstepping observer (blue, Section 4), a cathode PDE backstepping observer (yellow, Section 4), and a Padé-based boundary state observer (green, Section 5). (For interpretation of the references to color in this figure legend, the reader is referred to the web version of this article.)

$$w_x(0,t) = -\rho I(t), \tag{20}$$

$$w_x(1,t) = -\rho I(t), \tag{21}$$

$$y_e(t) = w(1,t) + \mu(t), \tag{22}$$

with function $f(w(x,t)) = (L^2/D_{\text{eff}})r(w(x,t))$ and $\rho = L/(2FAD_{Li^+})$. Note, $f(w(x,t))$ is globally Lipschitz continuous with respect to $w$ within $[c_{Li^+,\min}, c_{Li^+,\max}]$. The measured signal $y_e$ is the $Li^+$ concentration at electrolyte–cathode interface, where $\mu(t)$ denotes boundary measurement uncertainty in (22).

**Assumption 1.** The measurement error is bounded by $|\mu(t)| \le \bar{\mu}$, where $\bar{\mu} > 0$. The derivative of $\mu$ is bounded.

We hereby adopt the PDE backstepping concept which was initially developed for families of linear PDEs in Krstic and Smyshlyaev (2008) and later extended to certain classes of semilinear PDEs with disturbances (Mironchenko, Karafyllis, & Krstic, 2019; Zhang, Dey et al., 2021). Specifically, the observer is assembled based on a boundary state error injection:

$$\hat{w}_t = \hat{w}_{xx} + f(\hat{w}) + p_1(x)\left[y_e - \hat{w}(1)\right], \tag{23}$$

$$\hat{w}_x(0) = -\rho I, \tag{24}$$

$$\hat{w}_x(1) = -\rho I + p_{10}\left[y_e - \hat{w}(1)\right], \tag{25}$$

where $\hat{w}$ designates the estimation of $w$, and $p_1(x)$, $p_{10}$ are gains to be determined. Denote $\tilde{w} = w - \hat{w}$ the estimation error, governed by

$$\tilde{w}_t = \tilde{w}_{xx} + \phi - p_1(x)\tilde{w}(1) - p_1(x)\mu, \tag{26}$$

$$\tilde{w}_x(0) = 0, \tag{27}$$

$$\tilde{w}_x(1) = -p_{10}\tilde{w}(1) - p_{10}\mu, \tag{28}$$

where the nonlinear function $\phi$ in (26) is given by $\phi = f(w) - f(\hat{w})$. We seek a backstepping transformation

$$\tilde{w}(x,t) = \tilde{v}(x,t) - \int_x^1 K(x,\xi)\tilde{v}(\xi,t)\mathrm{d}\xi \tag{29}$$

to map the estimation error $\tilde{w}$ to a target system

$$\tilde{v}_t = \tilde{v}_{xx} + \psi - c\tilde{v} + g(x)\mu, \tag{30}$$

$$\tilde{v}_x(0) = 0, \tag{31}$$

$$\tilde{v}_x(1) = -c_1\tilde{v}(1) - p_{10}\mu. \tag{32}$$

In (29), $K(x,\xi)$ is the kernel function to be determined. The unknown coefficients $c$ and $c_1$ are tuning parameters, and $g(x)$ will be designed to ensure the invertibility of the backstepping transformation. Function $\psi(x,t)$ denotes the transformed version of $\phi(x,t)$ under the same backstepping transformation with kernel $K$,

$$\phi(x,t) = \psi(x,t) - \int_x^1 K(x,\xi)\psi(\xi,t)\mathrm{d}\xi. \tag{33}$$

The observer in (23)–(25) constitutes two vital challenges: (i) the nonlinearity in the PDE dynamics and (ii) the uncertainty in the boundary measurement. By differentiating the backstepping transformation, we discover the governing equations for the kernel function:

$$K_{xx}(x,\xi) - K_{\xi\xi}(x,\xi) = -cK(x,\xi), \tag{34}$$

$$K_x(0,\xi) = 0, \tag{35}$$

$$K(x,x) = -\frac{c}{2}x, \tag{36}$$

which leads to the observer gain functions:

$$p_1(x) = -K_\xi(x,1) - c_1K(x,1), \tag{37}$$

$$p_{10} = c_1 - K(1,1). \tag{38}$$

Via successive approximation, a unique closed-form solution exists for the kernel PDE (Krstic & Smyshlyaev, 2008, Chapter 4):

$$K(x,\xi) = -c\xi\frac{I_1\left(\sqrt{c(\xi^2-x^2)}\right)}{\sqrt{c(\xi^2-x^2)}}. \tag{39}$$

$I_1(\cdot)$ is the modified Bessel function of the first kind.

**Remark 2.** The existence and uniqueness of the inverse backstepping transformation

$$\tilde{v}(x,t) = \tilde{w}(x,t) + \int_x^1 \ell(x,\xi)\tilde{w}(\xi,t)\mathrm{d}\xi \tag{40}$$

can be established by differentiating both sides of (40) and by taking $g(x) = \ell_\xi(x,1)$ (Zhang, Dey et al., 2021). Coincidentally, the inverse backstepping kernel function $\ell(x,\xi)$ satisfies

$$\ell_{xx}(x,\xi) - \ell_{\xi\xi}(x,\xi) = c\ell(x,\xi), \tag{41}$$

$$\ell_x(0,\xi) = 0, \tag{42}$$

$$\ell(x,x) = -\frac{c}{2}x, \tag{43}$$

which has been proven to have a closed-form solution (Krstic & Smyshlyaev, 2008, Chapter 4).

Next, we introduce Lemma 1, whose proof is omitted here. A similar property has been established in Zhang, Dey et al. (2021).

**Lemma 1.** *The function $\psi$ is upper bounded by*

$$\|\psi(\cdot,t)\| \le \kappa(c,\gamma)\|\tilde{v}(\cdot,t)\|, \qquad \forall t \in [0,\infty), \tag{44}$$

*with $\kappa(c,\gamma) \triangleq \gamma[1+\rho(c)][1+\eta(c)]$, where*

$$\rho(c) \triangleq \sqrt{\int_0^1\int_x^1 \ell^2(x,\xi;c)\mathrm{d}\xi\mathrm{d}x}, \tag{45}$$

$$\eta(c) \triangleq \sqrt{\int_0^1\int_x^1 K^2(x,\xi;c)\mathrm{d}\xi\mathrm{d}x}. \tag{46}$$

*where $\gamma$ is a Lipschitz constant for function $f$.*

**Assumption 2.** The nonlinear function $f$ is globally Lipschitz with respect to $w$ within the range $[c_{\mathrm{Li}^+,\min}, c_{\mathrm{Li}^+,\max}]$. Further, the Lipschitz constant $\gamma$ satisfies $\gamma < 1.053$, a condition verified by the solid-state battery model with standard parameters.

**Theorem 1** (*Electrolyte Observer Convergence*)**.** *Under Assumptions 1–2 and Lemma 1, let $c$ and $c_1$ verify*

$$c + \frac{1}{4} - \kappa(c,\gamma) > 0, \qquad c_1 - \frac{1}{2} \ge 0. \tag{47}$$

*With the presence of boundary measurement error, i.e., $\mu(t) \neq 0$, the estimation error system is input-to-state stable (ISS) with respect to the disturbance $[\mu, \dot{\mu}]$.*

**Proof.** We recast the uncertainty from the boundary (32) to the in-domain dynamics via the transformation: $\tilde{v}(x,t) = z(x,t) - p_{10}\mu(t)(x^2-1)/2$, leading to

$$z_t = z_{xx} + \psi - cz + e_\mu, \tag{48}$$

$$z_x(0) = 0, \tag{49}$$

$$z_x(1) = -c_1z(1), \tag{50}$$

where $e_\mu(x,t) = [g(x) - p_{10}]\mu(t) + \frac{1}{2}p_{10}(x^2-1)[c\mu(t) + \dot{\mu}(t)]$. We consider the Lyapunov functional

$$W(t) = \frac{1}{2}\|z(\cdot,t)\|^2 = \frac{1}{2}\int_0^1 z^2(x,t)\mathrm{d}x, \tag{51}$$

whose derivative which produces

$$\dot{W} = -c_1z^2(1) - \|z_x\|^2 + \|z\|\|\psi\| - c\|z\|^2 + \|z\|\|e_\mu\|. \tag{52}$$

By Lemma 1, $\|\psi\| \le \kappa(c,\gamma)\left(\|z\| + p_{10}\bar{\mu}\|x^2-1\|/2\right)$. Moreover, $\|e_\mu\| \le \|g(x) - p_{10}\|\bar{\mu} + p_{10}\bar{U}\|x^2-1\|/2$, where $\bar{U} = \sup_t\{c\mu(t) + \dot{\mu}(t)\}$. Substitute $\|\psi\|$ and $\|e_\mu\|$ with their majorization and apply the Poincaré inequality,

$$\dot{W} \le -\left(c_1 - \frac{1}{2}\right)z^2(1) - p(c)\|z\|^2 + q(c,c_1)\|z\|, \tag{53}$$

with $p(c) = c - \kappa(c;\gamma) + 1/4$ and $q(c,c_1) = \|g(x) - p_{10}\|\bar{\mu} + p_{10}\|x^2-1\|\left[\bar{U} + \kappa(c;\gamma)\bar{\mu}/2\right]$.

Next, Assumption 2 ensures $p(c) > 0$. For a given Lipschitz constant $\gamma$, the exponential growth of $\kappa(c;\gamma)$ with respect to $c$ is evident due to the dependency on the modified Bessel function in the kernel $K(x,y)$. However, $p(c) > 0$ necessitate an affine function to dominate $\kappa(c;\gamma)$. A brief numerical study indicates that a feasible solution to $p(c) > 0$ is $\gamma < 1.053$.

When $p(c) > 0$ and $c_1 \ge 1/2$, (53) can be solved by the comparison principle (Khalil & Grizzle, 2002),

$$\|z(\cdot,t)\| \le \|z(\cdot,0)\|e^{-p(c)t} + \frac{q(c,c_1)}{p(c)}\left[1 - e^{-p(c)t}\right], \tag{54}$$

from which input-to-state stability with respect to measurement errors can be concluded, since the two terms on the right hand side of (54) are class $\mathcal{KL}$ and class $\mathcal{K}$ (Isidori, 1995), respectively, and $\lim_{t\to\infty}\|z(\cdot,t)\| = R_B = q(c,c_1)/p(c)$. Coupling with the invertibility of (29) completes the proof.

**Remark 3.** The ISS property leverages differentiability of the boundary disturbances with respect to time. Similar results have been demonstrated for linear parabolic systems (Argomedo, Witrant, & Prieur, 2012). Studies on ISS of linear parabolic PDEs without the need for differentiability of boundary disturbances include (Karafyllis & Krstic, 2016). Recent advancements addressed ISS of nonlinear parabolic PDEs with boundary disturbances, inspired by monotone control systems (Mironchenko et al., 2019).

Note that system (8)–(11) is a linear diffusion PDE whose observer design has been extensively explored, and we refer interested readers to Krstic and Smyshlyaev (2008).

## 5. Domain boundary state observer

The electrolyte and cathode state observers require the boundary states for error injection. These boundary states are practically not measured and must be inferred from voltage and current data (green block in Fig. 4). As previously discussed, the boundary states $c_{\text{Li}^+}(0,t)$, $c_{\text{Li}^+}(L,t)$, and $c_{\text{Lis}}(L,t)$ may not be uniquely identified by the voltage function (18), since the mappings are not one-to-one. Next, we investigate a frequency-domain approximation of the PDE models for discovering additional dynamics that the boundary states obey, which are then coupled with the voltage function to uniquely identify boundary states.

### 5.1. Electrolyte/cathode boundary state approximation

Assuming zero initial condition, the transfer function from $I$ to $c_{\text{Li}^+}(0,t)$ and $c_{\text{Li}^+}(L,t)$ can be obtained by applying Laplace transformation to Model B dynamics:

$$C_{\text{Li}^+}(0,s) = C^{\text{nh}}_{\text{Li}^+}(s) + C^{\text{h}}_{\text{Li}^+}(s), \tag{55}$$

$$C_{\text{Li}^+}(L,s) = C^{\text{nh}}_{\text{Li}^+}(s) - C^{\text{h}}_{\text{Li}^+}(s), \tag{56}$$

where

$$C^{\text{nh}}_{\text{Li}^+}(s) \triangleq \frac{\varepsilon}{s(s-\lambda)}, \tag{57}$$

$$C^{\text{h}}_{\text{Li}^+}(s) \triangleq \frac{I(s)}{2FAD_{\text{Li}^+}} \frac{\exp\left(\sqrt{\frac{s-\lambda}{D_e}}L\right) - 1}{\sqrt{\frac{s-\lambda}{D_e}}\left[\exp\left(\sqrt{\frac{s-\lambda}{D_e}}L\right) + 1\right]}. \tag{58}$$

The terms $C^{\text{nh}}_{\text{Li}^+}(s) = \mathcal{L}[c^{\text{nh}}_{\text{Li}^+}(t)]$ and $C^{\text{h}}_{\text{Li}^+}(s) = \mathcal{L}[c^{\text{h}}_{\text{Li}^+}(t)]$ encode the effects of non-homogeneous and homogeneous solutions, respectively. Since (55) and (56) are structurally similar with only a sign difference, we focus on the $y = 0$ case, and $y = L$ naturally follows.

We further define the following transfer functions,

$$G^{\text{nh}}_{\text{Li}^+}(s) \triangleq \frac{C^{\text{nh}}_{\text{Li}^+}(s)}{(\varepsilon/s)} = \frac{1}{s-\lambda}, \tag{59}$$

$$G^{\text{h}}_{\text{Li}^+}(s) \triangleq \frac{C^{\text{h}}_{\text{Li}^+}(s)}{I(s)} = \frac{1}{2FAD_{\text{Li}^+}} \times \frac{\exp\left(\sqrt{\frac{s-\lambda}{D_e}}L\right) - 1}{\sqrt{\frac{s-\lambda}{D_e}}\left[\exp\left(\sqrt{\frac{s-\lambda}{D_e}}L\right) + 1\right]}. \tag{60}$$

from the $\varepsilon$ to $c^{\text{nh}}_{\text{Li}^+}(t)$ and $I(t)$ to $c^{\text{h}}_{\text{Li}^+}(t)$, respectively. $G^{\text{nh}}_{\text{Li}^+}(s)$ can then be realized in time domain by low-pass filtering the constant signal $\varepsilon$ via

$$\dot{\chi}_0 = \lambda\chi_0 + \varepsilon, \quad y_{\text{nh}} = \chi_0, \tag{61}$$

where $\chi_0 \in \mathbb{R}$. Since $G^{\text{h}}_{\text{Li}^+}(s)$ is a nonlinear transcendental transfer function, we adopt Padé approximation (Forman, Bashash, Stein, & Fathy, 2010) to approximate it as a ratio of two power series of a given order $n$, $P_n(s)$. The order of the approximation can be dictated by the trade-off between computational burden and desired model accuracy. Fig. 5(a) and (b) depict the Bode plot of $G^{\text{h}}_{\text{Li}^+}(s)$ and its Padé approximations with various of orders. The approximates demonstrate fine performance under low frequencies, yet the accuracy deteriorates at high frequency ranges. Another feature is the superiority of higher order approximates to the lower ones. Given that 90% of the signal power from typical EV drive cycles is within frequencies less than 2.5 Hz (Marcicki, Canova, Conlisk, & Rizzoni, 2013), we choose a 3rd-order truncation to maintain the trade-off between accuracy and simplicity.

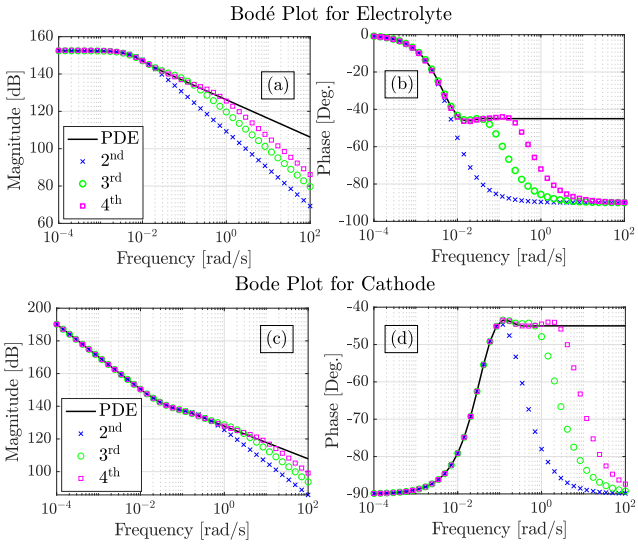


**Fig. 5.** (a), (b): Bode plots of the electrolyte transfer function (60) and Padé approximates up to 4th order. The model parameters are adopted from Danilov et al. (2010). (c), (d): Bode plots of the cathode transcendental transfer function (65) and Padé approximates up to 4th order.

Subsequently, the controllable canonical form is employed for the state-space realization of the 3rd-order Padé approximation for $G^{\text{h}}_{\text{Li}^+}(s)$, as follows,

$$\dot{\chi}_{\text{h}} = A_{\text{h}}\chi_{\text{h}} + B_{\text{h}}I, \quad y_{\text{h}} = C_{\text{h}}\chi_{\text{h}}, \tag{62}$$

where $\chi_{\text{h}} \in \mathbb{R}^3$. The values of $A_h$, $B_h$, and $C_h$ are not enumerated here, but can be inferred from the method of moment matching (Forman et al., 2010). Consequently, $y_{\text{h}}$ serves as an approximation of $c^{\text{h}}_{\text{Li}^+}(t)$, and the boundary states $c_{\text{Li}^+}(0,t)$ and $c_{\text{Li}^+}(L,t)$ can be approximated by

$$c_{\text{Li}^+}(0) = c^{\text{nh}}_{\text{Li}^+} + c^{\text{h}}_{\text{Li}^+} \approx y_{\text{nh}} + y_{\text{h}}, \tag{63}$$

$$c_{\text{Li}^+}(L) = c^{\text{nh}}_{\text{Li}^+} - c^{\text{h}}_{\text{Li}^+} \approx y_{\text{nh}} - y_{\text{h}}, \tag{64}$$

with sufficient accuracy, where $y_{\text{nh}}(t)$ and $y_{\text{h}}(t)$ are dynamically characterized by (61) and (62).

The preceding procedure can be applied to the cathode dynamics for its transcendental transfer functions,

$$G_{\text{Lis}}(0,s) = \frac{C_{\text{Lis}}(0,s)}{I(s)} = \frac{1}{FAD_{\text{Lis}}} \times \frac{\exp\left(2\sqrt{\frac{s}{D_{\text{Lis}}}}M\right) + 1}{\sqrt{\frac{s}{D_{\text{Lis}}}}\left[\exp\left(2\sqrt{\frac{s}{D_{\text{Lis}}}}M\right) - 1\right]}. \tag{65}$$

A Padé approximation is used to acquire a linear representation of (65). Fig. 5(c) and (d) provides the Bode plot of $G_{\text{Lis}}(0,s)$ alongside

Padé approximates up to 4th order. We elect to adopt the 3rd-order Padé approximant, whose controllable canonical form is realized by

$$\dot{\chi}_p = A_p\chi_p + B_p I, \quad c_{\text{Lis}}(L) = C_p\chi_p, \tag{66}$$

where $\chi_p \in \mathbb{R}^3$, and the method of moment matching can be used to derive the values of $A_p$, $B_p$, and $C_p$.

Our immediate goal is to come up with a state observer to uniquely estimate the boundary states of electrolyte and cathode, namely $c_{\text{Li}^+}(0,t)$, $c_{\text{Li}^+}(L,t)$, and $c_{\text{Lis}}(L,t)$, from voltage and current measurements.

### 5.2. Boundary state observer design and analysis

Let $\chi \triangleq [\chi_{\text{h}}^\top \;\; \chi_0 \;\; \chi_p^\top]^\top \in \mathbb{R}^7$ which satisfies

$$\dot{\chi} = A\chi + BI + B_2\varepsilon, \quad y_b = C\chi + h(\chi, I), \tag{67}$$

in which $A = \text{diag}(A_{\text{h}}, \lambda, A_p)$, $B = [(B_{\text{h}})^\top \;\; 0 \;\; B_p^\top]^\top$, and $B_2 = [0_{1\times 3} \;\; 1 \;\; 0_{1\times 3}]^\top$. $y_b$ encodes voltage, given by (18). We now design an observer based on (67) to reconstruct Li/Li$^+$ concentrations at domain boundaries:

$$\dot{\hat{\chi}} = A\hat{\chi} + BI + B_2\varepsilon + \tilde{L}\left[y_b - \hat{y}_b\right], \tag{68}$$

$$\hat{y}_b = C\hat{\chi} + h(\hat{\chi}, I), \tag{69}$$

in which $\hat{\chi}$ is the estimate of $\chi$ and observer gain $\tilde{L}$ is to be determined to establish observer convergence.

**Theorem 2** (*Boundary Observer Convergence*). *Suppose function $h(\chi, I)$ is Lipschitz continuous with respect to $\chi$, uniformly in $I$ with a Lipschitz constant $\nu$. Define the estimation error as $\tilde{\chi} = \chi - \hat{\chi}$. Then $\tilde{\chi}$ is asymptotically stable if $\tilde{L}$ can be chosen such that*

$$\begin{bmatrix} (A-\tilde{L}C)^\top P + P(A-\tilde{L}C) + \tau\nu^2\tilde{L}^\top\tilde{L}\mathbf{I} & P \\ P & -\tau\mathbf{I} \end{bmatrix} < 0 \tag{70}$$

*for some positive definite symmetric matrix $P$.*

**Proof.** The state estimation error system obeys

$$\dot{\tilde{\chi}} = (A-\tilde{L}C)\tilde{\chi} - \tilde{L}\left[h(\chi, I) - h(\hat{\chi}, I)\right]. \tag{71}$$

Using Lyapunov function candidate $V_b = \tilde{\chi}^\top P\tilde{\chi}$, where $P > 0$ is to be determined, its time derivative is

$$\dot{V}_b = \begin{bmatrix} \tilde{\chi}^\top & \Sigma^\top \end{bmatrix} \begin{bmatrix} (A-\tilde{L}C)^\top P + P(A-\tilde{L}C) & P \\ P & 0 \end{bmatrix} \begin{bmatrix} \tilde{\chi} \\ \Sigma \end{bmatrix}, \tag{72}$$

where $\Sigma(t) = -\tilde{L}\left[h(\chi, I) - h(\hat{\chi}, I)\right]$. Consider the Lipschitz continuous function $h(x, I)$ which satisfies

$$\left\|h(\chi, I) - h(\hat{\chi}, I)\right\|_2 \le \nu \left\|\chi - \hat{\chi}\right\|_2, \quad \forall \chi, \hat{\chi}. \tag{73}$$

We then have

$$\left[h(\chi, I) - h(\hat{\chi}, I)\right]^\top \left[h(\chi, I) - h(\hat{\chi}, I)\right] \le \nu^2\tilde{\chi}^\top\tilde{\chi}. \tag{74}$$

Multiplying both sides of (74) by $(\tilde{L}^\top\tilde{L})$ produces

$$\begin{bmatrix} \tilde{\chi}^\top & \Sigma^\top \end{bmatrix} \begin{bmatrix} -\nu^2\tilde{L}^\top\tilde{L}\mathbf{I} & 0 \\ 0 & \mathbf{I} \end{bmatrix} \begin{bmatrix} \tilde{\chi} \\ \Sigma \end{bmatrix} \le 0, \tag{75}$$

and $\mathbf{I}$ is an identity matrix. Applying the $\mathcal{S}$-procedure (Boyd, El Ghaoui, Feron, & Balakrishnan, 1994) to (72) and (75), we find $\dot{V}_b < 0$ if and only if there exists a $\tau \ge 0$ such that

$$\begin{bmatrix} (A-\tilde{L}C)^\top P + P(A-\tilde{L}C) + Q & P \\ P & -\tau\mathbf{I} \end{bmatrix} < 0, \tag{76}$$

where $Q = \tau\nu^2\tilde{L}^\top\tilde{L}\mathbf{I}$. Ultimately, the necessary and sufficient condition for the asymptotic convergence of the observer is given by $\exists\tau \ge 0$ such that (76) holds.

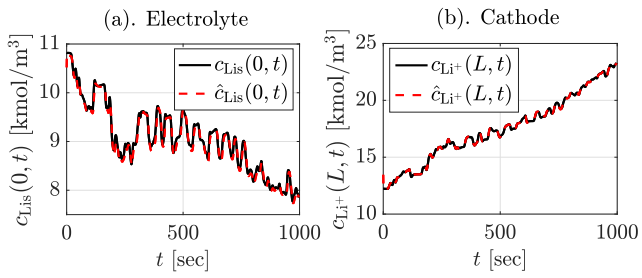


**Fig. 6.** The state estimation results from the boundary state observers.

**Remark 4.** The procedures for obtaining the solution $P$ and $\tilde{L}$ of (70) can be referred to Dey, Ayalew, and Pisu (2015), and Phanomchoeng and Rajamani (2010). Applying the Schur Inequality to Eq. (70), we arrive at the necessary and sufficient condition for the observer design:

$$(A-\tilde{L}C)^\top P + P(A-\tilde{L}C) + \tau G^\top G\mathbf{I} + \frac{1}{\tau}PP < 0, \tag{77}$$

in which $G = \nu\tilde{L}$. Corresponding to Theorem 2 in Phanomchoeng and Rajamani (2010), Eq. (77) can be re-written as

$$A^\top P + PA + \tau G^\top G\mathbf{I} + \frac{1}{\tau}PP - \beta^2 C^\top C < 0, \tag{78}$$

together with which one may choose the observer gain to be $\tilde{L} = \beta^2 P^{-1}C^\top/2$, in which $\beta$ can be freely assigned. Additionally, Eq. (78) can be modified into

$$A^\top P + PA + \tau G^\top G\mathbf{I} + \frac{1}{\tau}PP - \beta^2 C^\top C = -a\mathbf{I}, \tag{79}$$

where $a > 0$ is a small scalar. For given $\tau$, $\beta$, $a$, equation (79) can be solved numerically, which has been previously studied in Dey et al. (2015), and Phanomchoeng and Rajamani (2010).

## 6. Simulations

We now conduct simulation-based observer validation using on a 10 μAh planar thin-film solid-state battery (Danilov et al., 2010). Suppose the battery is in an equilibrium state with $c_{\text{Li}^+}(y, 0) = 10818$ mol/m$^3$ for all $y \in [0, L]$ and $c_{\text{Lis}}(y, 0) = 12232$ mol/m$^3$ for all $y \in [L, M]$. Meanwhile, the observers in the normalized coordinates are initialized at incorrect values with 15% of deviation from the true values: $\hat{w}(x, 0) = 0.85 \cdot c_{\text{Li}^+}(y, 0)$ and $\hat{u}(x, 0) = 1.15 \cdot c_{\text{Lis}}(y, 0)$ for all $x \in [0, 1]$. The performance of the observers is evaluated in the sense of $L_2$ spatial norm of estimation errors, and convergence time is defined as the time spent to reach within $\pm 20$ mol/m$^3$ band around zero. We apply a dynamic urban dynamometer driving schedule (UDDS) charge/discharge cycle. The maximum C-rate is 14.73 C, and the average C-rate is 2.72 C. This applied current load discharges the battery by roughly 91% in state of charge (SOC) within 20 min. High charge/discharge current rate is the main advantages of solid-state batteries against liquid electrolyte-based Li-ion batteries.

First, we examine the domain boundary state observer from Section 5. The boundary state observer is implemented based upon (68)–(69), and the equilibrium state $c_{\text{Li}^+}^{\text{eq}}$ for model linearization is around $c_{\text{Li}^+}^{\text{eq}} = c_{\text{Li}^+}(y, 0) = 10818$ mol/m$^3$. The boundary state observer gain $\tilde{L}$ is obtained by numerically solving (70). As such, the electrolyte and cathode boundary state estimates are visualized in Fig. 6(a) and (b) against their truth values obtained from the full-order model (Model A). Note the instant convergence, reinforced by the asymptotic convergence property in Theorem 2. It is also important to underline that the

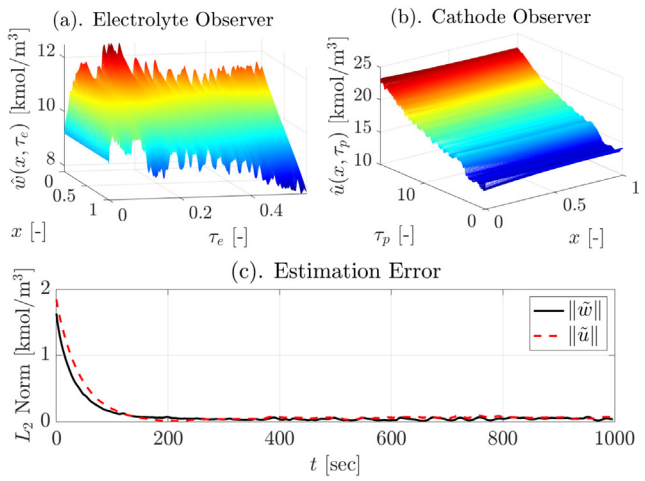


**Fig. 7.** The state observer performance for an UDDS drive cycle. The estimation errors exponentially converge to a ball around zero in the sense of spatial $L_2$ norm.

electrolyte boundary state observer in Fig. 6(a) maintains high estimation accuracy despite the states deviate from the equilibrium. Nevertheless, although insignificant, the estimation error stems from such a drift in the long term will propagate into the electrolyte lithium concentration observers subsequently. One practical method to mitigate this is to adaptively linearize the electrolyte model around the current state estimates. Finally, the boundary state estimates is received by the robust state observers as "boundary pseudo-measurements" for PDE backstepping. Fig. 7 presents the evolution of the state estimates, with the observer tuning parameters $c = 10$, $c_1 = 5$, $b = -1$, and $c_2 = -5$. Practically, a high gain (large $c$) produces faster observer convergence, whereas the estimation error bound $R_B$ expands monotonically with $c$. A clear trade-off exists that balances the convergence rate and sensitivity to noise. Note the spatial $L_2$ norm of the concentration estimation errors exhibit small bias. This bias is predominantly attributed to the estimation errors from the upstream boundary state observers. Exemplified by Theorem 1, the size of the bias can be controlled by the design parameters $c$ and $c_1$, Lipschitz constant $\gamma$, and the bound of boundary uncertainty.

## 7. Conclusion

As solid-state batteries demonstrate higher energy and power densities and ability for extreme fast charging, on-board energy management and accurate estimation of electrochemical states become a crucial task for safe and reliable operations. This paper presents a provably convergent state observer using a nonlinear electrochemical model. A PDE backstepping observer is developed to estimate electrolyte $Li^+$ concentration and cathode Li concentration relying on domain boundary states. These boundary states are rigorously obtained leveraging Padé approximations alongside an matrix-inequality-based nonlinear observer. Future research will investigate state estimation and optimal charging under coupled electrochemical and mechanical consideration to alleviate rapid degradation.

## References


Ahmad, Zeeshan, Hong, Zijian, & Viswanathan, Venkatasubramanian (2020). Design rules for liquid crystalline electrolytes for enabling dendrite-free lithium metal batteries. *Proceedings of the National Academy of Sciences*, *117*(43), 26672–26680.

Argomedo, Federico Bribiesca, Witrant, Emmanuel, & Prieur, Christophe (2012). D 1-input-to-state stability of a time-varying nonhomogeneous diffusive equation subject to boundary disturbances. In *2012 American control conference* (pp. 2978–2983). IEEE.

Behrou, Reza, & Maute, Kurt (2017). Numerical modeling of damage evolution phenomenon in solid-state lithium-ion batteries. *Journal of the Electrochemical Society*, *164*(12), A2573.

Boyd, Stephen, El Ghaoui, Laurent, Feron, Eric, & Balakrishnan, Venkataramanan (1994). *Linear matrix inequalities in system and control theory*. SIAM.

Danilov, D., Niessen, R. A. H., & Notten, PHL (2010). Modeling all-solid-state li-ion batteries. *Journal of the Electrochemical Society*, *158*(3), A215.

Deng, Zhongwei, Hu, Xiaosong, Lin, Xianke, Kim, Youngki, & Li, Jiacheng (2021). Sensitivity analysis and joint estimation of parameters and states for all-solid-state batteries. *IEEE Transactions on Transportation Electrification*.

Deng, Zhongwei, Hu, Xiaosong, Lin, Xianke, Xu, Le, Li, Jiacheng, & Guo, Wenchao (2020). A reduced-order electrochemical model for all-solid-state batteries. *IEEE Transactions on Transportation Electrification*.

Dey, Satadru, Ayalew, Beshah, & Pisu, Pierluigi (2015). Nonlinear robust observers for state-of-charge estimation of lithium-ion cells based on a reduced electrochemical model. *IEEE Transactions on Control Systems Technology*, *23*(5), 1935–1942.

Di Domenico, Domenico, Stefanopoulou, Anna, & Fiengo, Giovanni (2010). Lithium-ion battery state of charge and critical surface charge estimation using an electrochemical model-based extended Kalman filter. *Journal of Dynamic Systems, Measurement, and Control*, *132*(6).

Doyle, Marc, Fuller, Thomas F., & Newman, John (1993). Modeling of galvanostatic charge and discharge of the lithium/polymer/insertion cell. *Journal of the Electrochemical Society*, *140*(6), 1526.

Fabre, Steve D, Guy-Bouyssou, Delphine, Bouillon, Pierre, Le Cras, Frédéric, & Delacourt, Charles (2011). Charge/discharge simulation of an all-solid-state thin-film battery using a one-dimensional model. *Journal of the Electrochemical Society*, *159*(2), A104.

Forman, Joel C, Bashash, Saeid, Stein, Jeffrey L, & Fathy, Hosam K (2010). Reduction of an electrochemistry-based Li-ion battery model via quasi-linearization and Padé approximation. *Journal of the Electrochemical Society*, *158*(2), A93.

Hermann, Robert, & Krener, Arthur (1977). Nonlinear controllability and observability. *IEEE Transactions on Automatic Control*, *22*(5), 728–740.

Isidori, Alberto (1995). *Nonlinear control systems*. Springer London.

Janek, Jürgen, & Zeier, Wolfgang G. (2023). Challenges in speeding up solid-state battery development. *Nature Energy*, *8*(3), 230–240.

Karafyllis, Iasson, & Krstic, Miroslav (2016). ISS with respect to boundary disturbances for 1-D parabolic PDEs. *IEEE Transactions on Automatic Control*, *61*(12), 3712–3724.

Kazemi, Namdar, Danilov, Dmitri L, Haverkate, Lucas, Dudney, Nancy J, Unnikrishnan, Sandeep, & Notten, Peter HL (2019). Modeling of all-solid-state thin-film li-ion batteries: Accuracy improvement. *Solid State Ionics*, *334*, 111–116.

Khalil, Hassan K., & Grizzle, Jessy W. (2002). *Vol. 3, Nonlinear systems*. Prentice hall Upper Saddle River, NJ.

Kim, Youngki, Lin, Xianke, Abbasalinejad, Armin, Kim, Sun Ung, & Chung, Seung Hyun (2019). On state estimation of all solid-state batteries. *Electrochimica Acta*, *317*, 663–672.

Koga, Shumon, Camacho-Solorio, Leobardo, & Krstic, Miroslav (2021). State estimation for lithium-ion batteries with phase transition materials via boundary observers. *Journal of Dynamic Systems, Measurement, and Control*, *143*(4).

Krstic, Miroslav, & Smyshlyaev, Andrey (2008). *Boundary control of PDEs: A course on backstepping designs*. SIAM.

Marcicki, James, Canova, Marcello, Conlisk, A Terrence, & Rizzoni, Giorgio (2013). Design and parametrization analysis of a reduced-order electrochemical model of graphite/LiFePO4 cells for SOC/SOH estimation. *Journal of Power Sources*, *237*, 310–324.

Mironchenko, Andrii, Karafyllis, Iasson, & Krstic, Miroslav (2019). Monotonicity methods for input-to-state stability of nonlinear parabolic PDEs with boundary disturbances. *SIAM Journal on Control and Optimization*, *57*(1), 510–532.

Moura, Scott J, Argomedo, Federico Bribiesca, Klein, Reinhardt, Mirtabatabaei, Anahita, & Krstic, Miroslav (2016). Battery state estimation for a single particle model with electrolyte dynamics. *IEEE Transactions on Control Systems Technology*, *25*(2), 453–468.

Phanomchoeng, Gridsada, & Rajamani, Rajesh (2010). Observer design for Lipschitz nonlinear systems using Riccati equations. In *Proceedings of the 2010 American control conference* (pp. 6060–6065). IEEE.

Raijmakers, L. H. J., Danilov, D. L., Eichel, R. A., & Notten, P. H. L. (2020). An advanced all-solid-state Li-ion battery model. *Electrochimica Acta*, *330*, Article 135147.

Upreti, Kushagra, Oyewole, Isaiah, Lin, Xianke, & Kim, Youngki (2019). On simplification of a solid-state battery model for state estimation. In *2019 IEEE conference on control technology and applications* (pp. 487–492). IEEE.

Zhang, Dong, Couto, Luis D., & Moura, Scott J. (2020). Electrode-level state estimation in lithium-ion batteries via Kalman decomposition. *IEEE Control Systems Letters*, *5*(5), 1657–1662.
Zhang, Dong, Dey, Satadru, Tang, Shu-Xia, Drummond, Ross, & Moura, Scott J. (2021). Battery internal temperature estimation via a semilinear thermal PDE model. *Automatica*, *133*, Article 109849.
Zhang, Dong, Tang, Shu-Xia, Couto, Luis D, & Viswanathan, Venkatasubramanian (2021). PDE observer for all-solid-state batteries via an electrochemical model. In *2021 IEEE conference on control technology and applications* (pp. 51–56). IEEE.

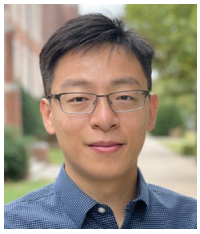

**Dong Zhang** received the B.S. degree in civil and environmental engineering from the University of Michigan, Ann Arbor, MI, USA, in 2015, the B.S. degree in electrical and computer engineering from Shanghai Jiao Tong University, Shanghai, China, in 2015, and the M.S. and Ph.D. degrees in systems and control engineering from the University of California at Berkeley, Berkeley, CA, USA, in 2016 and 2020, respectively. He is currently an Assistant Professor in aerospace and mechanical engineering at The University of Oklahoma, Norman, OK, USA. His current research interests include dynamical system estimation and controls, optimization, machine learning, renewable energy systems, energy storage, and advanced lithium-ion battery management systems.

Dr. Zhang was a recipient of the American Society of Mechanical Engineers (ASME) Energy System Best Paper Award and the Finalist at the 2020 American Control Conference (ACC) and the 2020 Dynamic Systems and Control Conference (DSCC).

**Shu-Xia Tang** received her Ph.D. in Mechanical Engineering in 2016 from the Department of Mechanical & Aerospace Engineering, University of California, San Diego, USA. She is currently an assistant professor at the Department of Mechanical Engineering, Texas Tech University, USA. She is an IEEE senior member and is an IEEE CSS (Control Systems Society) Technical Committee member on Distributed Parameter Systems. She serves as the editor of ASME (American Society of Mechanical Engineers) Dynamic Systems and Control Division (DSCD) Newsletter and serves as an Editorial Board member of IEEE CSS and ASME DSCD. Her main research interests are stability analysis, estimation and control design of distributed parameter systems including swarm robotic systems and energy storage systems.

**Luis D. Couto** received the bachelor's degree in chemical engineering from Simón Bolívar University, Caracas, Venezuela, in 2013, the master's degree in renewable energies from the Autonomous University of Madrid, Madrid, Spain, in 2014, and the Ph.D. degree from the Free University of Brussels, Ixelles, Belgium, in 2018. In 2020, he was a Visiting Scholar at the Department of Engineering Science, University of Oxford, Oxford, U.K. In 2022, he was a Post-Doctoral Researcher with the Department of Control Engineering and System Analysis, Free University of Brussels. He is currently a Researcher in electrical energy storage at the Unit Energy Technology, VITO, Flemish Institute for Technological Research, Mol, Belgium. His current research interests include state/parameter estimation, fault diagnosis, and optimal control in the context of battery management systems.

**Zhongbao Wei** received the B.E. and M.S. degrees in instrumental science and technology from Beihang University, Beijing, China, in 2010 and 2013, respectively, and the Ph.D. degree in power engineering from Nanyang Technological University, Singapore, in 2017. He is currently a Professor with the National Engineering Laboratory for Electric Vehicles, Beijing Institute of Technology, Beijing, China. His research interests include electrified transportation and battery management. Dr. Wei serves as an Associate Editor for many international journals such as IEEE TRANSACTIONS ON INDUSTRIAL ELECTRONICS and IEEE TRANSACTIONS ON INTELLIGENT TRANSPORTATION SYSTEMS.

**Venkatasubramanian Viswanathan** received his Ph.D. degree from Stanford University in 2013 and the B.S. degree from Indian Institute of Technology Madras in 2008. He is currently an associate professor in the Department of Mechanical Engineering at Carnegie Mellon University. His research focuses on material design for electrochemical energy systems with specific applications, including Li-ion and Li-metal batteries, autonomous experimentation, and battery electrolytes.

He is the recipient of several awards, including the Office of Naval Research Young Investigator Award in 2019, Sloan Research Fellowship in Chemistry in 2018, the National Science Foundation CAREER award in 2016, the American Chemical Society PRF Young Investigator Award in 2014, and the Electrochemical Society Daniel Cubicciotti Award in 2010.